Spatiotemporal dynamics of Kerr-Raman optical frequency combs

Yanne K. Chembo,[1,*] Ivan S. Grudinin,[2] and Nan Yu[2]
[1]*Institut FEMTO-ST, CNRS–Université Bourgogne Franche-Comté, Département d'Optique, 15B Avenue des Montboucons, 25030 Besançon cedex, France*
[2]*Jet Propulsion Laboratory, California Institute of Technology, 4800 Oak Grove Drive, Pasadena, California 91109, USA*
(Received 19 November 2014; published 14 October 2015)

Optical frequency combs generated with ultrahigh-Q whispering-gallery-mode resonators are expected to provide a compact, versatile, and energy-efficient source for the generation of coherent lightwave and microwave signals. So far, Kerr and Raman nonlinearities in these resonators have predominantly been investigated separately, even though both effects originate from the same third-order susceptibility. We present a spatiotemporal formalism for the theoretical understanding of these Kerr-Raman combs, which allows us to describe the complex interplay between both nonlinearities and all-order dispersion. These theoretical findings are successfully compared with experiments performed with ultrahigh-Q calcium and magnesium fluoride resonators.

DOI: 10.1103/PhysRevA.92.043818 PACS number(s): 42.65.Sf, 42.65.Hw, 42.65.Ky

The study of nonlinear phenomena in whispering-gallery-mode (WGM) resonators has been the focus of intense research activities in recent years. These resonators are generally characterized by ultrahigh quality factors, which enable efficient light-matter interactions between the long-lifetime photons and the nonlinear host material. The main result of this interaction is a frequency-mixing process that depletes the continuous-wave pump and populates the quasiequidistant eigenmodes of the resonator, thereby generating signals with new optical frequencies when certain conditions are met. A plethora of applications is expected to benefit from these compact multiwavelength sources, particularly in the areas of metrology, sensing, aerospace, and communication engineering.

In amorphous media or centrosymmetric crystals, the leading nonlinear effects are related to the third-order susceptibility $\chi^{(3)}$. In this case, the light-matter interaction in the WGM resonator generally yields either a Kerr or a Raman comb when the resonator is pumped above a certain threshold. On the one hand, Kerr combs are highly coherent and originate from the quasi-instantaneous electronic response of the bulk medium to the laser excitation. Kerr combs have been extensively studied and are known to display a very wide variety of spatiotemporal dynamical behaviors, such as Turing patterns, spatiotemporal chaos, cavity solitons, and breathers [1–13]. Adjacent side modes can be symmetrically excited regardless of their spectral distance from the pump (typically, few GHz). On the other hand, Raman combs result from the delayed molecular response of the host medium to the laser excitation. These combs are generally incoherent and result from the cascaded excitation of longer wavelength modes—or Stokes lines—far away from the pump, typically at 10 THz and its harmonics [14–19].

Despite originating from the same nonlinear susceptibility, and the fact that both effects are most of the time excited simultaneously, Kerr and Raman effects in WGM resonators have almost always been investigated separately. The investigation of the interplay between Kerr and Raman has been considered only very recently [20–23], but it remains to a large extent unexplored. In fact, one should also consider the critical role of dispersion at all orders in this case, since the very large action range of Raman scattering forbids the crude approximation that consists of considering only low-order dispersion coefficients. This situation is indeed similar to the one of super-continuum generation, where the complex interplay between Kerr, Raman, and all-order dispersion leads to the dramatic spectral broadening of short and powerful pulses launched in highly nonlinear crystal fibers [24]. The standard model used in supercontinuum generation can therefore be adapted to our case, provided that some critical features specific to WGM resonators are accounted for. Indeed, the most important difference is that our system has periodic boundary conditions. This is a feature that can lead to several nontrivial consequences from the mathematical, physical, and numerical analysis standpoints. Another important peculiarity of this system is the existence of stationary solutions, resulting from the balance between pump power and losses, and between dispersion and $\chi^{(3)}$ nonlinearity. Along that line, the spatiotemporal dynamics of dissipative structures in optical cavities is known to be substantially different from the one of optical impulsions propagating in a fiber [25]. Therefore, totally unexpected stationary states are likely to emerge in WGM resonators when both Kerr and Raman nonlinearities are excited.

In this paper, we present a spatiotemporal formalism to investigate this interaction between Kerr, Raman, and all-order dispersion effects in WGM resonators. We consider a WGM resonator of principal radius a and frequency-dependent refractive index $n(\omega)$. This partial differential equation (PDE) model describing the spatiotemporal dynamics of the intracavity field obeys

$$\frac{\partial \mathcal{E}}{\partial t} = -\frac{1}{2}\Delta\omega_{\rm tot}\mathcal{E} + i\sigma\mathcal{E} + iv_g\sum_{k=2}^{+\infty}(i\Omega_{\rm FSR})^k\frac{\beta_k}{k!}\frac{\partial^k\mathcal{E}}{\partial\theta^k} + \sqrt{\frac{\Delta\omega_{\rm ext}}{T_{\rm FSR}}}\sqrt{P_{\rm L}} + iv_g\gamma\left[1+\frac{\Omega_{\rm FSR}}{\omega_{\rm L}}\frac{\partial}{\partial\theta}\right]\times\left[\mathcal{E}(\theta,t)\int_{-\pi}^{\pi}R(\theta'/\Omega_{\rm FSR})\,|\mathcal{E}(\theta-\theta',t)|^2\,d\theta'\right], \quad (1)$$

*yanne.chembo@femto-st.fr

where t is the time, $\theta \in [-\pi,\pi]$ is the azimuthal angle along the rim of the disk, and the intracavity field $\mathcal{E}(\theta,t)$ in the moving frame is normalized in a way that $|\mathcal{E}|^2$ directly yields the optical power in watts.

The first term in the right-hand side stands for the intrinsic and extrinsic (or coupling) losses, characterized by the total linewidth $\Delta\omega_{\rm tot} = \omega_{\rm c}/Q_{\rm tot}$, where $Q_{\rm tot}$ is the loaded quality factor. The second term in the right-hand side stands for the effect of the off-resonance pumping, since the parameter $\sigma = \omega_{\rm L} - \omega_{\rm c}$ is the detuning of the angular laser frequency with respect to cold-cavity resonance of the pumped mode. The third term in the right-hand side accounts for both the material and geometrical dispersion at all orders ($k \geqslant 2$): in fact, accounting for higher-order dispersion coefficients β_k becomes here mandatory because the Raman gain is shifted up to multiple tens of THz away from the pump. The chromatic dispersion can be accurately determined using the Sellmeier expansion of $n(\omega)$ [26,27], while the contribution of geometrical dispersion can be calculated from the approximation of spherical resonators, which is accurate for disk-resonators with curvature radii significantly larger than the pump wavelength. The fourth term in the right-hand side stands for the external pumping term, which depends on the external Q-factor through $\Delta\omega_{\rm ext}$, on the intracavity round-trip time $T_{\rm FSR} = 2\pi/\Omega_{\rm FSR}$, and of course, on the optical power $P_{\rm L}$ of the pump. Finally, the nonlinear effects induced by the $\chi^{(3)}$ susceptibility are gathered in the fifth term. The Kerr nonlinear term is here proportional to the nonlinear coefficient $\gamma = \omega_{\rm L} n_2/cA_{\rm eff}$, where $\omega_{\rm L}$ is the pump frequency, n_2 is the nonlinear optical coefficient [proportional to $\chi^{(3)}$], and $A_{\rm eff}$ is the effective mode area inside the resonator. It is generally difficult to evaluate exactly the mode area in WGM resonators, but a good estimate in our case is given by $A_{\rm eff} \simeq 0.35\,[\lambda_{\rm L}/n_g]^{\frac{7}{6}} a^{\frac{5}{6}}$, where $\lambda_{\rm L}$ is the pump wavelength [28]. The perturbation operator $[\Omega_{\rm FSR}/\omega_{\rm L}]\,\partial_\theta$ accounts for eventual shock phenomena induced by self-steepening. The time-domain behavior of the nonlinear host material is ruled by the impulse response $R(t) = [1 - f_{\rm R}]\delta(t) + f_{\rm R} h_{\rm R}(t)$, where the first term in the right-hand side stands for the Kerr effect (quasi-instantaneous electronic response), while the second accounts for the Raman effect (delayed molecular response). In the latter case, the impulse response corresponding to the Raman gain is $h_{\rm R}(t)$. By setting $f_{\rm R}$ to zero and neglecting the shock term, we obtain the Lugiato-Lefever equation [29] that has been used to model Kerr comb generation [30–32] and which has already been proven to be a very fruitful and accurate formalism for the understanding of these combs [33–35]. In the present work, we model the Raman gain $g(\Omega)$ as a Lorentzian line shape of peak value $g_{\rm R}$, center frequency $\Omega_{\rm R}$ and FWHM line width $\Delta\Omega_{\rm R}$, so that the fractional impulse response explicitly reads

$$h_{\rm R}(t) = H(t)\,\frac{\tau_1^2 + \tau_2^2}{\tau_1 \tau_2^2}\, e^{t/\tau_2} \sin(t/\tau_1), \qquad (2)$$

where $\tau_1 = 1/\Omega_{\rm R}$, $\tau_2 = 2/\Delta\Omega_{\rm R}$, and $H(t)$ is the Heaviside step function. The fractional coefficient can be calculated as

$$f_{\rm R} = \frac{c}{\pi \omega_{\rm L} n_2(\omega_{\rm L})} \int_0^{+\infty} dt \int_0^{+\infty} d\Omega\, g(\Omega) \sin(\Omega t)\,, \qquad (3)$$

where $\omega_{\rm L}$ is the pump frequency.

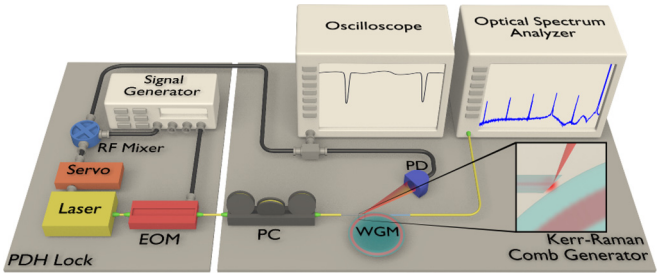

FIG. 1. (Color online) Schematical representation of the experimental setup. A crystalline CaF_2 or MgF_2 WGM resonator is pumped by a continuous-wave laser, and the coupling is ensured by angle-polished optical fibers. The reflected output signal is detected by a photodetector (PD) and monitored with a fast oscilloscope, while the transmitted signal in the drop port is directly monitored by an optical spectrum analyzer. The Pound-Drever-Hall (PDH) stabilization loop using an electro-optical modulator (EOM) was needed to lock the 1064-nm pump laser to the CaF_2 resonator. The polarization controller (PC) was inserted after the 1560-nm laser pumping the MgF_2 resonator.

The principal characteristics of Raman response for fluorite crystals results from experimental and theoretical works in condensed matter physics. Calcium fluoride has a cubic fluorite structure O_h^1 with three atoms per unit cell. It has a single (degenerated) Raman-active phonon branch with F_{2g} symmetry, shifted at 322 $\rm cm^{-1}$ with line width 15 $\rm cm^{-1}$. In the frequency domain, it corresponds to a Stokes resonance shifted at $\Omega_{\rm R}/2\pi = 9.66$ THz, with a full-width at half-maximum (FWHM) line width $\Delta\Omega_{\rm R}/2\pi = 450$ GHz at room temperature. At 1064 nm, the Kerr nonlinearity coefficient is equal to $n_2 = 3 \times 10^{-20}\rm W/m^2$. Magnesium fluoride has tetragonal rutile structure D_{4h}^{14} with two atoms per unit cell. From group theory, it can be shown that it has four first-order Raman-active branches, known in the nomenclature as A_{1g} (Γ_1^+), B_{1g} (Γ_3^+), B_{2g} (Γ_4^+), and E_{1g} (Γ_5^-). Generally, the strongest response is provided by the phonon branch A_{1g}, shifted at 410 $\rm cm^{-1}$ with line width 7 $\rm cm^{-1}$ ($\Omega_{\rm R}/2\pi = 12.3$ THz and $\Delta\Omega_{\rm R}/2\pi = 210$ GHz at room temperature). The Kerr nonlinearity at 1560 nm is $n_2 = 0.9 \times 10^{-20}\rm W/m^2$. For both CaF_2 and MgF_2, the crystal orientation and cut, as well as the polarization of the pump, have an influence on the Raman branches that are excited in the system. It is also noteworthy that in both cases, the Raman gain has a relatively high quality factor $Q_{\rm R} = \Omega_{\rm R}/\Delta\Omega_{\rm R}$ (of the order of few tens), while it is significantly lower in optical fibers ($Q_{\rm R} \simeq 1/2$).

The experimental system is presented in Fig. 1. A crystalline WGM disk-resonator is pumped using a continuous-wave laser. The pump laser radiation is coupled inside the resonator using the evanescent field of an angle-polished optical fiber. The crystals are either CaF_2 or MgF_2 disk resonators with size ranging from a few hundred microns to a few millimeters, and with intrinsic quality factors of the order of 10^9 at 1550 nm. The free beam reflected from the resonator is photodetected, and the generated electric signal is eventually fed back to the laser via a Pound-Drever-Hall lock, which stabilizes the laser frequency to the pumped cavity resonance, or through thermal self-stabilization.

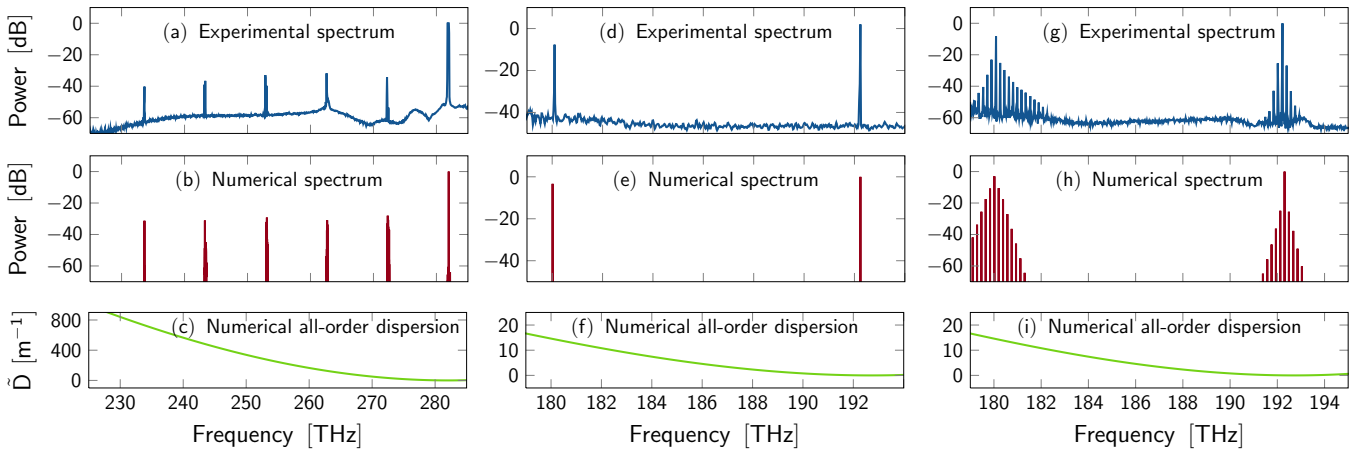

FIG. 2. (Color online) Comparison between experimental and simulated spectra, along with the all-order dispersion curves. (a) Raman excitation for the CaF_2 resonator pumped at 1064 nm (∼282 THz). (b) Corresponding numerical simulation with $P_L = 1\,\mu$W and $\sigma = 0$. (c) Corresponding dispersion curve. (d) Raman excitation for the MgF_2 resonator pumped at 1560 nm (∼192 THz). (e) Corresponding numerical simulation with $P_L = 5\,\mu$W and $\sigma = -\Delta\omega_{tot}/2$. (f) Corresponding dispersion curve. (g) Kerr-Raman excitation for the MgF_2 resonator pumped at 1560 nm (∼192 THz). (h) Corresponding numerical simulation with $P_L = 18\,\mu$W and $\sigma = -\Delta\omega_{tot}/2$. (i) Corresponding dispersion curve.

We first investigate the spatiotemporal dynamics of the system when the cavity is a CaF_2 resonator with radius $a = 5$ mm, and pumped at 1064 nm and with $Q_{in} = 5 \times 10^9$. Above a given threshold pump value, the intracavity spatiotemporal dynamics shows that after a transient time, Stokes lines are sequentially excited, at up to the fifth order. However, in the time domain, no asymptotic state is reached, thereby indicating that the comb is essentially incoherent. Figures 2(a) and 2(b) display a comparison between the theoretical and experimental combs. Since the Raman gain is shifted at $\Omega_R/2\pi = 9.66$ THz away from the pump, the overall spectral span of this comb is therefore of around 50 THz, and the model agrees with the experimental data over this large frequency range, where the dispersion is found to be strongly normal. The bandwidth of the Raman gain (∼450 GHz) is much larger than the free-spectral range of the resonator (∼13 GHz), and as a consequence, several modes are typically excited for each order of the Raman scattering. The second configuration under study is with a MgF_2 disk-resonator with main radius $a = 190\,\mu$m, and pumped at 1560 nm. Figure 2(c) shows a spectrum where a Raman line has been excited in the resonator. This excited mode is shifted at ∼12.3 THz from the carrier as expected. The numerical simulation also shows that this regime, which corresponds to very low pump powers, can also be described by the generalized Eq. (1). However, as the power is increased, we find that there is a regime where both Kerr and Raman effects are simultaneously excited, as displayed in Fig. 2(g). In this regime, the dispersion is found to be only weakly normal, and the comb displays a highly stable output (local coherence) as shown in the spectrotemporal representation of Fig. 3. This regime is similar to the one presented in Ref. [20], where it was shown that the comb around the Stokes Raman line was coherent. The local coherence of this Kerr-Raman comb is lost when the power is further increased, and a wide but nonstationary comb can be obtained when the resonator is pumped beyond mW intracavity power.

An exhaustive analytical study of Eq. (1) is indeed very difficult to achieve because of the many degrees of freedom that are involved. However, our numerical simulations presented in Figs. 2 provides insightful understanding of the effect of dispersion and pump power on the formation of Kerr-Raman combs. Even though it logically appears that both Kerr and Raman effects are simultaneously excited when the pump power is high enough, we find that all-order dispersion plays a critical role as far as local coherence is concerned. Our results indicate that optimal conditions to obtain a high degree of local coherence combines a pump above Raman threshold (same order of magnitude) and a weak all-order normal dispersion, as evidenced in Fig. 2.

In conclusion, we have described a unified formalism for the theoretical description of Kerr-Raman frequency combs. Results of the numerical simulations of Eq. (1) agree very well with the corresponding experimental measurements, demonstrating the accuracy of the proposed theoretical model. It is noteworthy that dispersion plays a critical role in Kerr-Raman comb generation, which arise in the regime of weakly normal all-order dispersion. The model can be

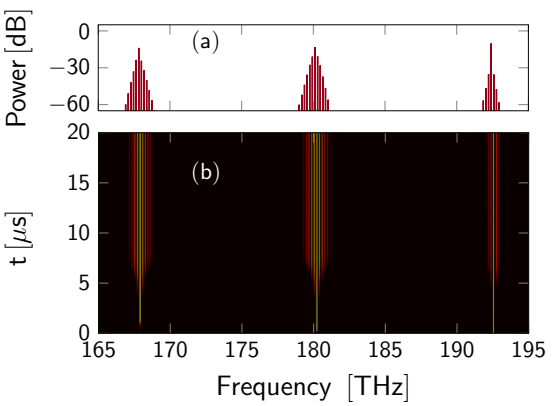

FIG. 3. (Color online) Spectrotemporal dynamics of the locally coherent Kerr-Raman comb of Fig. 2(h). The asymptotic power spectrum is displayed in (a), while the spectrotemporal dynamics of the Kerr-Raman comb is shown in (b).

improved by accounting for intracavity thermal effects, which are expected to play a critical role on the nature of the comb, along with the cavity detuning. We expect that dispersion management will provide useful degrees of freedom for the purpose of tailoring these combs for many applications [36].

Y.K.C. acknowledges financial support from the European Research Council through the projects NextPhase (ERC StG Grant No. 278616) and Versyt (ERC PoC Grant No. 632108), from the *Centre National d'Etudes Spatiales* (CNES) through the project SHYRO, from the *Région de Franche-Comté*, and from the LabEx ACTION. He acknowledges hospitality at the NASA Jet Propulsion Laboratory as a Visiting Scientist during the completion of this research work. This work was performed at the Jet Propulsion Laboratory, California Institute of Technology, under a contract with NASA.

[1] P. Del'Haye, A. Schliesser, O. Arcizet, T. Wilken, R. Holzwarth, and T. J. Kippenberg, Nature **450**, 1214 (2007).
[2] Y. K. Chembo, D. V. Strekalov, and N. Yu, Phys. Rev. Lett. **104**, 103902 (2010).
[3] Y. K. Chembo and N. Yu, Phys. Rev. A **82**, 033801 (2010).
[4] T. J. Kippenberg, R. Holzwarth, and S. A. Diddams, Science **332**, 555 (2011).
[5] F. Ferdous, H. Miao, D. E. Leaird, K. Srinivasan, J. Wang, L. Chen, L. T. Varghese and A. M. Weiner, Nature Photon. **5**, 770 (2011).
[6] A. A. Savchenkov, A. B. Matsko, W. Liang, V. S. Ilchenko, D. Seidel, and L. Maleki, Nature Photon. **5**, 293 (2011).
[7] P. Del'Haye, S. B. Papp, and S. A. Diddams, Phys. Rev. Lett. **109**, 263901 (2012).
[8] T. Herr, K. Hartinger, J. Riemensberger, C. Y. Wang, E. Gavartin, R. Holzwarth, M. L. Gorodetsky, and T. J. Kippenberg, Nature Photon. **6**, 480 (2012).
[9] J. Li, H. Lee, T. Chen, and K. J. Vahala, Phys. Rev. Lett. **109**, 233901 (2012).
[10] J. Pfeifle *et al.*, Nature Photon. **8**, 375 (2014).
[11] J. Pfeifle *et al.*, Phys. Rev. Lett. **114**, 093902 (2015).
[12] T. Herr, V. Brasch, J. D. Jost, C. Y. Wang, N. M. Kondratiev, M. L. Gorodetsky, and T. J. Kippenberg, Nature Photon. **8**, 145 (2014).
[13] C. Godey, I. V. Balakireva, A. Coillet, and Y. K. Chembo, Phys. Rev. A **89**, 063814 (2014),
[14] S. M. Spillane, T. J. Kippenberg, and K. J. Vahala, Nature **415**, 621 (2002).
[15] B. Min, T. J. Kippenberg, and K. J. Vahala, Opt. Lett. **28**, 1507 (2003).
[16] T. J. Kippenberg, S. M. Spillane, D. K. Armani, and K. J. Vahala, Opt. Lett. **29**, 1224 (2004).
[17] T. J. Kippenberg, S. M. Spillane, B. Min, and K. J. Vahala, IEEE J. Sel. Top. Quantum Electron. **10**, 1219 (2004).
[18] I. S. Grudinin and L. Maleki, Opt. Lett. **32**, 166 (2007).
[19] I. S. Grudinin and L. Maleki, J. Opt. Soc. Am. B **25**, 594 (2008).
[20] W. Liang, V. S. Ilchenko, A. A. Savchenkov, A. B. Matsko, D. Seidel, and L. Maleki, Phys. Rev. Lett. **105**, 143903 (2010).
[21] I. S. Grudinin, L. Baumgartel, and N. Yu, Opt. Express **20**, 6604 (2012).
[22] I. S. Grudinin, L. Baumgartel, and N. Yu, Opt. Express **21**, 26929 (2013).
[23] L. Zhang, A. M. Agarwal, L. C. Kimerling, and J. Michel, Proc. SPIE **8960**, 896004 (2014).
[24] J. M. Dudley, G. Genty, and S. Coen, Rev. Mod. Phys. **78**, 1135 (2006).
[25] P. Grelu and N. Akhmediev, Nature Photon. **6**, 84 (2012).
[26] M. Daimon and A. Masumura, Appl. Opt. **41**, 5275 (2002).
[27] M. J. Dodge, Appl. Opt. **23**, 1980 (1984).
[28] V. B. Braginsky, M. L. Gorodetsky, and V. S. Ilchenko, Phys. Lett. A **137**, 393 (1989).
[29] L. A. Lugiato and R. Lefever, Phys. Rev. Lett. **58**, 2209 (1987).
[30] A. B. Matsko, A. A. Savchenkov, W. Liang, V. S. Ilchenko, D. Seidel, and L. Maleki, Opt. Lett. **36**, 2845 (2011).
[31] Y. K. Chembo and C. R. Menyuk, Phys. Rev. A **87**, 053852 (2013).
[32] S. Coen, H. G. Randle, T. Sylvestre, and M. Erkintalo, Opt. Lett. **38**, 37 (2013).
[33] A. Coillet, I. Balakireva, R. Henriet, K. Saleh, L. Larger, J. M. Dudley, C. R. Menyuk, and Y. K. Chembo, IEEE Photon. J. **5**, 6100409 (2013).
[34] A. Coillet and Y. K. Chembo, Opt. Lett. **39**, 1529 (2014).
[35] A. Coillet and Y. K. Chembo, Chaos **24**, 013113 (2014).
[36] I. S. Grudinin and N. Yu, Optica **2**, 221 (2015)